Various refined theories applied to damped viscoelastic beams and circular rings

M. Filippi[a*], E. Carrera[a†]

[a] Department of Mechanical and Aerospace Engineering, Politecnico di Torino, Corso Duca degli Abruzzi 24, 10129, Torino, Italy.

Abstract

In this work, a number of enhanced finite beam elements has been tested considering layered structures with viscoelastic layers. The viscoelastic properties have been defined with the complex modulus approach, and the equations of motion have been derived using the Principle of Virtual Displacement. Higher-order theories, based on equivalent-single layer and the layer-wise approaches, have been obtained with the Carrera Unified Formulation, which makes it possible to generate an infinite number of kinematic approximations. Both Lagrange-type elements and higher-order zig-zag theories have been developed within the layer-wise approach. On the other hand, Taylor-like expansions and Murakami-type zig-zag functions have been used to conceive the equivalent-single layer models. Numerical simulations have been performed considering symmetric and asymmetric laminated structures with rectangular and circular cross-sections. The results are reported in terms of frequencies, modal loss factors and frequency responses. The obtained results have been compared with solutions published in the literature and with solid finite element models. The accuracy of the different formulations has been found to be problem-dependent to a great extent.

Keywords: CUF; FEM; Viscoelasticity; Layer-wise approach; Equivalent-single layer approach

*Postdoctoral Research Fellow, e-mail: matteo.filippi@polito.it

†Professor of Aerospace Structures and Aeroelasticity, e-mail: erasmo.carrera@polito.it

1. Introduction

Viscoelastic materials (VEMs) are used in many engineering fields (aerospace, automotive, biomechanics, etc.) for the passive control of vibration amplitudes. VEMs exhibit characteristics that fall somewhere between elastic solids and viscous fluids with a low weight, which enable a part of the energy to be dissipated during dynamic deformations. The VEM stress-strain relation is defined using relaxation functions that are expressed with complex quantities in the frequency domain. The values of complex moduli, which are functions of the temperature and the frequency, are usually interpolated through inverse techniques, using a limited number of experimental data [1–3]. The problem is intrinsically nonlinear, and its solution requires dedicated solving techniques, such as the modal strain energy technique [4, 5], the direct frequency response method [6], the complex iterative eigensolution [7], or the asymptotic solution method [8, 9]. From a practical point of view, one of the most weight-effective ways of exploiting the damping capabilities is to incorporate viscoelastic materials between stiffer layers (Constrained-Layer Damping), which have the purpose of ensuring the required overall stiffness. Over the years, various theories have been developed to correctly predict the dynamic behavior of such structures. As far as analytical approaches are concerned, Kerwin [10] solved the vibrational problem for simply-supported or infinitely long viscoelastic beams. Other theoretical solutions have been proposed considering symmetric and asymmetric three-layer configurations with different boundary conditions, in order to extend Kerwin's theory [11–14]. In these works, the shear effects of the constraining layers have been neglected, and the shear motion of the core has been considered as the only damping mechanism. Durocher

and Solecki [15] derived a fourth-order equation for analyzing symmetric three-layer plates in which the shear deformation of elastic layers and rotatory inertia were included. On the other hand, Douglas [16] and Sisemore and Darvennes [17] developed dedicated analytical models in order to demonstrate the importance of transverse compressional damping. The comparisons with experimental data revealed that models based on the shear mechanism might lead to inaccurate results when stubby beams and thick viscoelastic cores were considered. Consequently, Xie and Shepard [18] proposed an enhanced beam formulation that encompassed shear, longitudinal extension, and transverse compression in the core layer. By conducting parametric studies on various three-layer structures, the authors were able to determine the relative contributions of the different damping mechanisms. The results demonstrated the importance of compressional damping, especially for off-resonance conditions, whereas the contribution of longitudinal extension seemed to be negligible throughout the considered frequency range. Other analytical approaches have been conceived for the study of beams with multiple constrained layer damping patches [19], circular plates [20], and rings [21]. Although these methodologies have provided interesting insights on the dynamics of damped structures, the need for techniques that are able to model more complex configurations has led to an extensive use of finite elements. Many researchers have developed beam [3, 9, 22, 23] and plate [8, 24] finite elements using the Euler-Bernoulli (or Kirchoff-Love) kinematics for stiffer layers, and first-order shear deformation theories (Timoshenko or Reissner-Mindlin models) for the soft core. Although these approximations can yield accurate results in many cases, they imply that the structure does not experience significant strains or stresses associated with the thickness direction. Therefore, several higher-order theories have been proposed

to overcome this limitation. For example, Treviso *et al.* [25] evaluated the capabilities of a refined zig-zag theory by performing a number of analysis on thick viscoelastic beams. Korjakin *et al.* [26] developed a two-dimensional finite element with 54 degrees of freedom to predict the dynamic response of sandwich revolution shells. With the same scope, Chazot *et al.* [27], and Kpeky *et al.* [28] proposed a multilayered element based on the P-order shear deformation theory with an added first-order zig-zag function and with a solid-shell formulation, respectively. Ferreira *et al.* [7] and Plagianakos and Saravanos [29] instead developed higher-order elements based on the layer-wise approach.

This paper has the aim of comparing different finite beam elements. Higher-order 1D theories have been obtained through the Carrera Unified Formulation (CUF), which makes it possible to automatically conceive an infinite number of kinematic models. In particular, theories based on the equivalent-single layer (ESL) and the layer-wise (LW) approach have been evaluated, considering different structural problems, including symmetric and asymmetric laminated rectangular beams and layered rings. Besides Lagrange-type expansions, which were previously tested in a study on viscoelastic structures [30], higher-order zig-zag theories, based on Taylor-like series of cross-sectional coordinates, [31] have been evaluated within the LW framework. As far as the ESL approach is concerned, the Murakami zig-zag function has been added to Taylor-like expansions. The results have been reported in terms of frequencies, modal loss factors and frequency response, and they have been compared with FE numerical solutions and with results available in the literature. The paper is organized as follows: Section 2 contains the preliminaries pertaining to the viscoelastic problem; Section 3 presents the considered kinematic assumptions; Section 4 is devoted to the numerical results, and the

concluding remarks are given in Section 5.

2. Governing equations

The general form of the Principle of Virtual Displacements (PVD) establishes the well-known relation between the kinematically admissible perturbations (indicated by δ) of the strain energy (L_{int}), inertial energy (L_{ine}), and the external work (L_{ext}) exerted by the forces ($\tilde{\boldsymbol{F}}$):

$$\delta L_{int} = \delta L_{ext} + \delta L_{ine} \tag{1}$$

The energies of Eq. 1 can be expressed in terms of the displacement vector, $\boldsymbol{u}^T = [u_x, u_y, u_z]$, as it follows

$$\int_V \delta \boldsymbol{u}^T \boldsymbol{D}^T \boldsymbol{C} \boldsymbol{D} \boldsymbol{u} \, dV = \int_V \delta \boldsymbol{u}^T \tilde{\boldsymbol{F}} \, dV + \int_V \delta \boldsymbol{u}^T \rho \ddot{\boldsymbol{u}} \, dV \tag{2}$$

where ρ is the material density, and $\ddot{\boldsymbol{u}}$ is the acceleration vector. The matrices $\boldsymbol{D}$ and $\boldsymbol{C}$, whose explicit forms can be found in [32], are the operators of the linear strain-displacement equations and the constitutive law that are reported in Eq. 3

$$\boldsymbol{\epsilon} = \boldsymbol{D}\,\boldsymbol{u} \qquad \boldsymbol{\sigma} = \boldsymbol{C}\,\boldsymbol{\epsilon} \tag{3}$$

in which $\boldsymbol{\epsilon}$ and $\boldsymbol{\sigma}$ denote the strain and stress vectors, respectively. According to the complex modulus approach, the engineering moduli are being defined as complex quantities

$$E(i\omega) = E_{c0}(\omega) * (1 + i\eta_c(\omega)) \tag{4}$$

with i=$\sqrt{-1}$. The storage modulus E_{c0}, and the corresponding material loss factor η_c are functions of the vibration frequency 'ω'.

The fundamental CUF equation is based on a simple separation of variables, according to which, the 3D displacement field $\boldsymbol{u}(x, y, z, t)$ is being assumed to be a combination of products between cross-sectional functions F_τ(x,z), and the generalized displacement vector $\boldsymbol{u}_\tau$(y,t)

$$\boldsymbol{u}(x, y, z, t) = F_\tau(x, z)\boldsymbol{u}_\tau(y, t) \qquad \tau = 1, 2, \ldots, M \tag{5}$$

The subscript τ stands for summation, and M is the number of terms in the expansion. The F_τ(x,z) functions are assumed $a - priori$, and the generalized displacement vector along the beam axis is interpolated through a classical finite element technique

$$\mathbf{u}_\tau(y, t) = N_i(y)\mathbf{q}_{\tau i}(t) \tag{6}$$

where $\mathbf{q}_{\tau i}^T(t) = [q_{u_{x_{\tau i}}}, q_{u_{y_{\tau i}}}, q_{u_{z_{\tau i}}}]$ is the nodal displacement vector, and N_i are the lagrangian shape functions along the longitudinal axis (see [32] (§5.2.2)). To obtain the variational statement in CUF form, Eqs. 5, 6 and 3 are substituted in Eq. 2

$$\delta \boldsymbol{q}_{\tau i}^T \int_V F_\tau N_i \boldsymbol{D}^T \boldsymbol{C} \boldsymbol{D} F_s N_j \, dV \, \boldsymbol{q}_{sj} \;=\; \delta \boldsymbol{q}_{\tau i}^T \int_V F_\tau N_i \, \tilde{\boldsymbol{F}} \, dV + \delta \boldsymbol{q}_{\tau i}^T \int_V F_\tau N_i \boldsymbol{I} \rho F_s N_j \, dV \, \ddot{\boldsymbol{q}}_{sj} \tag{7}$$

where $\boldsymbol{I}$ is the 3-by-3 identity matrix. The variational principle of Eq. 7 is satisfied for all possible perturbations if the following equations of motion are fulfilled

$$\boldsymbol{M}^{ij\tau s}\ddot{\boldsymbol{q}}_{sj} + \boldsymbol{K}^{ij\tau s}\boldsymbol{q}_{sj} = \boldsymbol{F}^{i\tau} \tag{8}$$

The matrix $\boldsymbol{M}^{ij\tau s}$ is the real-valued mass matrix, $\boldsymbol{K}^{ij\tau s}$ is the complex stiffness matrix, and $\boldsymbol{F}^{i\tau}$ is the loading vector expressed in terms of *fundamental nuclei*. The dimension of the stiffness and the mass matrix is 3-by-3, while $\boldsymbol{F}$ is a 3-by-1 vector. The complete structural tensors ($\boldsymbol{M}$, $\boldsymbol{K}$, and $\boldsymbol{F}$) related to the adopted mathematical model are obtained using a classical assembly technique. Homogeneous equations of motion are solved assuming a periodic solution in order to determine the complex eigenvalues ($\Lambda^* = \Lambda + i\,\Lambda'$), and corresponding eigenvectors ($\bar{\mathbf{q}}$) of the system

$$(-\Lambda^* \boldsymbol{M} + \boldsymbol{K}(\omega))\,\bar{\mathbf{q}} = 0 \tag{9}$$

The $n-$th damped frequency is related to the real part of the $n-$th complex eigenvalue ($\omega_n = \sqrt{\Lambda_n}$), while the modal loss factor is defined as $\eta_n{=}(\Lambda'_n)/(\Lambda_n)$. For the frequency response analysis, the load is assumed harmonic $\boldsymbol{F} = \bar{\boldsymbol{F}}_0 e^{i\omega t}$ and the Eq.10 is solved for a range of frequencies 'ω'

$$\left(-\omega^2 \boldsymbol{M} + \boldsymbol{K}(\omega)\right)\bar{\mathbf{q}} = \bar{\boldsymbol{F}}_0 \tag{10}$$

The unified formulation makes it possible to generate and compare an infinite, at least theoretically, number of different theories since the governing equations are systematically obtained from Eq. 2 regardless of which kinematic assumptions are adopted.

3. Kinematic assumptions

Let us consider a laminated structure with a prismatic cross-section constituted of n layers. The cross-section is ideally divided into K subdomains including one or more layers, which have the thickness and the width equal to $h_k = z_{k-1} - z_k$ and b, respectively (see Fig. 1).

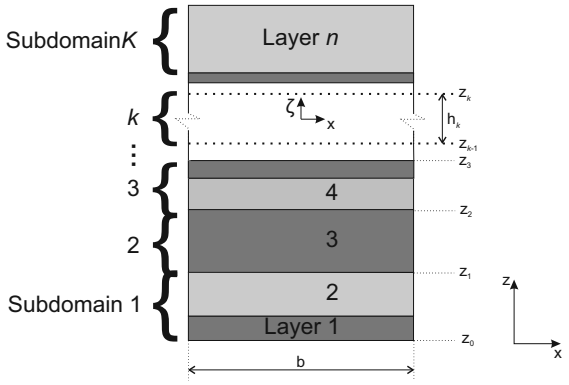

Figure 1: Cross-section of a laminated structure.

Such a structure can be analysed using equivalent single-layer approaches or layer-wise techniques. In the following sections, the two methodologies, and the corresponding kinematic assumptions, are outlined.

3.1. Equivalent-single layer approaches

Within the ESL context, 2D Taylor-like expansions are used to generate the N-th order beam theories (hereafter referred as TEN). Equation 11 shows an example of the refined displacement model up to the second order (TE2)

$$\begin{aligned} u_x &= u_{x_1} + x\, u_{x_2} + z\, u_{x_3} + x^2\, u_{x_4} + xz\, u_{x_5} + z^2\, u_{x_6} \\ u_y &= u_{y_1} + x\, u_{y_2} + z\, u_{y_3} + x^2\, u_{y_4} + xz\, u_{y_5} + z^2\, u_{y_6} \\ u_z &= u_{z_1} + x\, u_{z_2} + z\, u_{z_3} + x^2\, u_{z_4} + xz\, u_{z_5} + z^2\, u_{z_6} \end{aligned} \tag{11}$$

The terms over the linear ones represent the warping of the section, higher the number of terms, more flexible is the cross-section. Euler-Bernoulli and Timoshenko models can be obtained as particular cases of the linear expansion, TE1. Murakami [34] introduced his function in the first order shear deformation theory to fulfill the C_{z0} requirement for laminated structures. Hereafter, the theories that contain the Murakami term are identified with the superscript (Mzz). For example, the previous second-order theory with the Murakami zig-zag function becomes ($TE2^{Mzz}$)

$$
\begin{aligned}
u_x &= u_{x_1} + x\ u_{x_2} + z\ u_{x_3} + x^2\ u_{x_4} + xz\ u_{x_5} + z^2\ u_{x_6} + (-1)^k \frac{2\zeta_k}{h_k} u_{x_{7Z}} \\
u_y &= u_{y_1} + x\ u_{y_2} + z\ u_{y_3} + x^2\ u_{y_4} + xz\ u_{y_5} + z^2\ u_{y_6} + (-1)^k \frac{2\zeta_k}{h_k} u_{y_{7Z}} \\
u_z &= u_{z_1} + x\ u_{z_2} + z\ u_{z_3} + x^2\ u_{z_4} + xz\ u_{z_5} + z^2\ u_{z_6} + (-1)^k \frac{2\zeta_k}{h_k} u_{z_{7Z}}
\end{aligned}
$$

where ζ_k is the subdomain thickness coordinate, which ranges from $-h_k/2$ to $h_k/2$, and h_k is the thickness of the $k-layer$. It is well-known that the Mzz function is linear, and its value varies from -1 to 1 within each layer. The slope is, therefore, inversely proportional to the layer thickness. Based on the Murakami's idea, a warping zig-zag function is here proposed in order to describe deformations that occur in case of torsion

$$
F_\tau = (-1)^k \frac{4x\zeta_k}{bh_k}
$$

The x-coordinate ranges from -b/2 to b/2. The kinematic models that encompass the warping zig-zag term are labeled with the subscript $(wMzz)$. Figure

2 graphically shows the zig-zag functions defined over a cross-section with three layers.

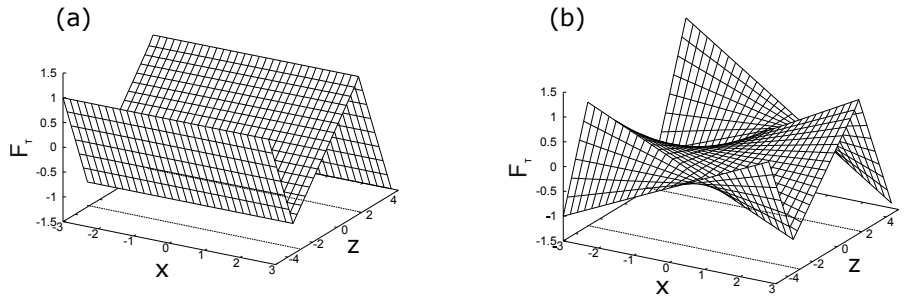

Figure 2: (a) Murakami zig-zag function and (b) warping zig-zag function defined above a three-layer cross-section.

3.2. Layer-wise approach

3.2.1. Layer-wise models with higher-order zig-zag functions

In order to overcome the limitations of the ESL approaches, the variable kinematic field can be written by using an arbitrary number of continuous piecewise polynomial functions, which are defined over the entire cross-section. The p_k-order polynomial expansion of the generic subdomain k is a combination of power functions of the section coordinates. Assuming that the mechanical properties vary discretely along the thickness direction, the F_τ functions defined over the k-th subdomain are

$$F_\tau(x,z)_k^{(p_x,p_z)} = \begin{cases} (-1)^{p_z}\left(\frac{2x}{b}\right)^{p_x}, & \text{if } \mathrm{z} < \mathrm{z_{k-1}} \\ (1)\left(\frac{2x}{b}\right)^{p_x}\left(\frac{2\zeta}{h_k}\right)^{p_z}, & \text{if } \mathrm{z_{k-1}} < \mathrm{z} < \mathrm{z_k} \\ (1)^{p_z}\left(\frac{2x}{b}\right)^{p_x}, & \text{if } \mathrm{z} > \mathrm{z_k} \end{cases} \tag{12}$$

where the superscripts p_x, p_z are the polynomial orders. The polynomial orders can be arbitrarily assumed for each subdomain. Moreover, the F_τ functions are

defined such that they range from -1 and +1 regardless on which polynomial orders (p_x, p_z) are considered [31]. Owing to the zig-zag form of these displacement fields, first derivatives with respect to the thickness direction, $\mathrm{F}_{\tau,z}$, are discontinuous. It is noteworthy that, depending on the number of considered subdomains K, the proposed methodology can represent either an equivalent single layer approach (K=1) or a "pure" layer-wise kinematic model (K=n). Such expansions are being denoted with the following notation

- TE-LW(p_c): the subscript 'c' indicates that the 'p'-th order expansion is used for each subdomain. If the number of subdomains does not coincide with the number of structural layers, the superscript (*) is added to the notation (TE-LW(p_c)*);
- TE-LW($p_1 - p_2 - \ldots - p_K$): the local expansion order of each subdomain 'p_k' is explicitly reported in brackets starting from the bottom surface.

According to this notation, two expressions of the first component of the displacement field (u_x) are reported below for a 2-subdomain structure (see Eq. 12)

- TE-LW(2_c):

$$\begin{aligned} u_x \;=\; & 1\,u_{x1} + F_\tau(x,z)_1^{(1,0)}\,u_{x2} + F_\tau(x,z)_1^{(0,1)}\,u_{x3} + F_\tau(x,z)_2^{(0,1)}\,u_{x4} + F_\tau(x,z)_1^{(2,0)}\,u_{x5} + \\ & + F_\tau(x,z)_1^{(1,1)}\,u_{x6} + F_\tau(x,z)_1^{(0,2)}\,u_{x7} + F_\tau(x,z)_2^{(1,1)}\,u_{x8} + F_\tau(x,z)_2^{(0,2)}\,u_{x9} \end{aligned}$$

- TE-LW(1-2):

$$\begin{aligned} u_x \;=\; & 1\,u_{x1} + F_\tau(x,z)_1^{(1,0)}\,u_{x2} + F_\tau(x,z)_1^{(0,1)}\,u_{x3} + F_\tau(x,z)_2^{(0,1)}\,u_{x4} + F_\tau(x,z)_2^{(2,0)}\,u_{x5} + \\ & + F_\tau(x,z)_2^{(1,1)}\,u_{x6} + F_\tau(x,z)_2^{(0,2)}\,u_{x7} \end{aligned}$$

where u_{x1}, u_{x2}, ..., u_{xN} are the theory unknowns. It should be observed that the functions $F_\tau(x,z)_k^{(p_x,0)}$ appear only once in the expansions since they coincide for all subdomains.

3.2.2. Lagrange-like Expansions

The second layer-wise model exploits the capabilities of the Lagrange-like expansions (denoted as LE). The cross-section is being discretized using two-dimensional Lagrangian elements with an arbitrary number of points. Moreover, the isoparametric formulation is used to deal with arbitrary shape geometries. For the nine-point element (LE9), for example, the interpolation functions are given by

$$F_\tau = \tfrac{1}{4}(r^2 + r\ r_\tau)(s^2 + s\ s_\tau) \qquad \tau = 1,3,5,7$$

$$F_\tau = \tfrac{1}{2}s_\tau^2(s^2 - s\ s_\tau)(1 - r^2) + \tfrac{1}{2}r_\tau^2(r^2 - r\ r_\tau)(1 - s^2) \qquad \tau = 2,4,6,8 \tag{13}$$

$$F_\tau = (1 - r^2)(1 - s^2) \qquad \tau = 9$$

where r and s vary from -1 to $+1$, whereas r_τ and s_τ are the coordinates of the nine points in the natural coordinate frame (see Fig. 3).

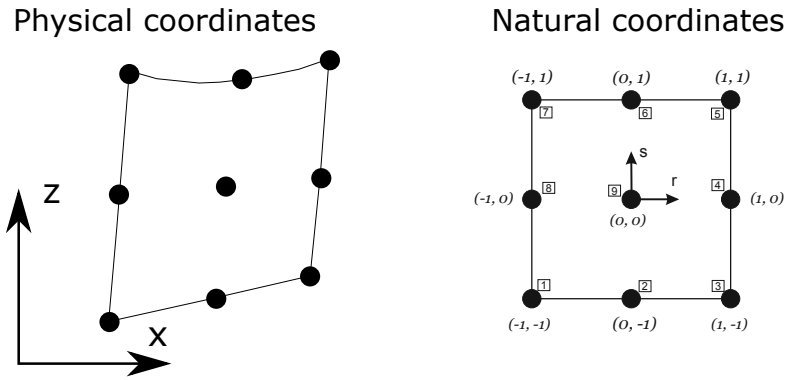

Figure 3: Coordinates mapping between coordinate systems

The corresponding displacement field is

$$\begin{aligned} u_x &= F_1\, u_{x_1} + F_2\, u_{x_2} + F_3\, u_{x_3} + ... + F_9\, u_{x_9} \\ u_y &= F_1\, u_{y_1} + F_2\, u_{y_2} + F_3\, u_{y_3} + ... + F_9\, u_{y_9} \\ u_z &= F_1\, u_{z_1} + F_2\, u_{z_2} + F_3\, u_{z_3} + ... + F_9\, u_{z_9} \end{aligned} \tag{14}$$

where $u_{x_1}, ..., u_{z_9}$ are the displacement variables, and they are the translational displacement components of each elemental point. For more details on Lagrange 1D models, the authors suggest to refer to [35] and [36], where Lagrange elements with 3, 4, 6 and 16 nodes were described.

4. Numerical results and discussion

4.1. Thin core damped beam

A rectangular cross section sandwich beam with metallic face sheets and a viscoelastic core is considered. The structure is cantilevered and has a length $L =$ 177.8 mm, width $b = 12.7$ mm and height $h = 3.175$ mm. The face sheets have equal thicknesses $h_1 = h_3 = 1.524$ mm, while the thickness of the core is $h_2 = 0.127$ mm. The properties of the metallic material are: Young's modulus $E_f = 69$ GPa,

density $\rho_f = 2766$ kg/m^3 and Poisson's ratio $\nu_f = 0.3$. The core is made of ISD 468 material with shear modulus $G_c = 0.69$ MPa, density $\rho_c = 968.1$ kg/m^3, and Poisson's ratio $\nu_c = 0.3$. Since the viscoelastic material is isotropic, the assumed Young's modulus of the core is $E_c = \frac{G_c}{2(1+\nu_c)}$. The loss factor of the core has been assumed constant, $\eta_c = 1$. Numerical simulations have been performed using a mathematical model consisting of 8 4-node beam elements along the longitudinal axis. The first 6 flexural and 2 torsional frequencies, with the corresponding loss factors, are shown in Tabs. 1 and 2 where a converged 3D finite element solution, and the results presented in [9] and [8], are reported for comparison purposes. The results have revealed that, if the zig-zag term is not included in the expansions, the ESL theories are not able to adequately detect the flexural and torsional behaviour of the beam. The frequency values are in fact very far from the reference solutions (see Tab. 1), while the loss factors (not reported) are equal to zero, regardless of which mode shapes and theory orders are considered. On the other hand, the Murakami zig-zag function has determined significant improvements in the solutions, in terms of frequencies and loss factors related to the flexural mode shapes. The same consideration can be made for the warping zig-zag function, which has led to a relevant reduction in the discrepancies between the 1D results and the 3D-FE solution for the torsional modes. As far as LW techniques are concerned, the Lagrange-type expansions have been able to reproduce the reference results with significant accuracy. Complete as well as reduced expansions have been tested for the TE-LW theories. It can be observed that convergence of the results has been achieved by adopting the third-order expansion, that is, TE-LW(3_c).

Figure 4 shows the axial (v^*) and transverse (w^*) displacement components related to the first and second bending mode shapes. Each mode shape was obtained

	f_1	f_2	f_3	f_4	f_5	f_6	f_7^+	f_8^+	DOFs
Ref. [9]	67.5	303.1	749.4	1398.3	2266.3	3350.9	-	-	-
Ref. [8]	67.8	309.1	761.1	1420.6	2297.9	3395.9	-	-	-
3D FE	68.234	306.577	756.839	1414.78	2304.44	3432.11	1001.90	3028.85	7128
				ESL theories					
TE2	82.699	517.593	1446.95	2829.61	4666.37	6953.30	2105.05	6330.52	450
TE4	82.649	517.147	1444.97	2823.58	4651.93	6923.92	2009.52	6040.28	1125
TE7	82.626	516.983	1444.34	2821.83	4647.94	6916.13	1986.72	5971.78	2700
				ESL theories with Maurakami-type functions					
TE2^{Mzz}	68.916	322.037	816.354	1540.68	2509.89	3720.58	2008.14	4634.13	525
TE2^{Mzz}_{wMzz}	68.654	313.622	782.545	1471.42	2400.83	3572.58	1037.87	3147.43	600
TE4^{Mzz}	68.647	316.529	795.209	1494.58	2429.95	3597.65	1925.26	4533.26	1200
TE4^{Mzz}_{wMzz}	68.426	310.048	768.887	1437.74	2335.36	3461.82	1026.28	3109.43	1275
TE7^{Mzz}	68.530	314.194	786.170	1474.62	2395.20	3545.23	1905.72	4514.64	2775
TE7^{Mzz}_{wMzz}	68.344	308.796	764.154	1426.83	2315.40	3429.48	1021.30	3091.33	2850
				LW theories					
3LE16	68.206	306.695	756.284	1409.04	2283.52	3378.84	1017.13	3078.48	3000
3LE9	68.213	306.748	756.465	1409.53	2284.65	3381.14	1034.58	3130.85	1575
TE-LW(1_c)	72.999	337.531	849.517	1599.10	2600.27	3850.51	4325.80	12977.3	375
TE-LW(1-2-1)	71.861	336.345	849.195	1598.91	2600.18	3850.43	4214.25	13020.0	600
TE-LW(2_c)	68.324	307.477	759.339	1417.85	2303.09	3414.88	1036.12	3138.85	900
TE-LW(2-3-2)	68.319	307.475	759.338	1417.85	2303.09	3414.88	1035.38	3135.14	1200
TE-LW(3_c)	68.212	306.731	756.377	1409.24	2283.94	3379.66	1034.53	3130.57	1650
TE-LW(3-4-3)	68.211	306.727	756.367	1409.23	2283.91	3379.62	1034.38	3129.76	2025
TE-LW(4_c)	68.195	306.629	756.110	1408.68	2282.84	3377.56	1019.28	3084.89	2625

'+': torsional frequencies.

'−': result not provided by the theory.

Table 1: Damped frequencies [Hz] for the three-layer isotropic beam.

	η_1	η_2	η_3	η_4	η_5	η_6	η_7^+	η_8^+
Ref. [9]	0.202	0.218	0.150	0.088	0.057	0.039	-	-
Ref. [8]	0.204	0.201	0.142	0.086	0.057	0.037	-	-
3D FE	0.200	0.214	0.147	0.085	0.054	0.035	0.015	0.015
ESL theories with Maurakami-type functions								
TE2^{Mzz}	0.186	0.177	0.112	0.063	0.040	0.027	0.074	0.292
TE2^{Mzz}_{wMzz}	0.195	0.202	0.134	0.077	0.049	0.033	0.014	0.015
TE4^{Mzz}	0.192	0.190	0.123	0.070	0.045	0.030	0.067	0.276
TE4^{Mzz}_{wMzz}	0.198	0.209	0.142	0.082	0.053	0.036	0.014	0.015
TE7^{Mzz}	0.194	0.196	0.129	0.074	0.047	0.032	0.066	0.272
TE7^{Mzz}_{wMzz}	0.200	0.212	0.144	0.084	0.054	0.037	0.014	0.015
LW theories								
3LE16	0.198	0.212	0.148	0.087	0.056	0.038	0.015	0.015
3LE9	0.198	0.212	0.147	0.087	0.056	0.038	0.014	0.015
TE-LW(1_c)	0.194	0.186	0.119	0.068	0.043	0.029	0.000	0.000
TE-LW(1-2-1)	0.180	0.180	0.117	0.067	0.043	0.029	0.008	0.037
TE-LW(2_c)	0.201	0.216	0.148	0.086	0.055	0.037	0.014	0.015
TE-LW(2-3-2)	0.201	0.216	0.148	0.086	0.055	0.037	0.014	0.015
TE-LW(3_c)	0.202	0.217	0.149	0.087	0.056	0.038	0.014	0.015
TE-LW(3-4-3)	0.202	0.217	0.149	0.087	0.056	0.038	0.014	0.015
TE-LW(4_c)	0.202	0.217	0.149	0.087	0.056	0.038	0.015	0.015

'$^+$': torsional loss factor.

'$-$': result not provided by the theory.

Table 2: Modal loss factors [-] for the three-layer isotropic beam.

from the real and imaginary parts of the corresponding eigenvector, which was normalized with respect to its maximum complex modulus. The current results are compared with the mode shapes obtained from the 3D-FE solution. The LW approach and the ESL theories with the Murakami's term were able to describe the zig-zag distributions of the axial displacement, which are shown in Figs. 4-b and 4-d, in spite of the relevant transversal anisotropy.

4.2. Thick core damped beam

Flexural and torsional vibration amplitudes have been evaluated by means of direct frequency analyses, which have been performed on a cantilever viscoelastic beam with a thick viscoelastic core. The structure has a rectangular cross-section, in which the thicknesses of the face sheets and the core are h_f =0.40624 mm and h_c =6.3475 mm, respectively and the length-to-width ratio, L/b, is assumed to be 5 (b = 25.4 mm). The mechanical properties of the structural face sheets and the core are: Young's moduli E_f = 68.9 GPa, E_c = 179.14 MPa, densities ρ_f = 2687.3, ρ_c = 119.69 kg/m^3, and Poisson's ratios $\nu_f = \nu_c = 0.3$. In order to deal with slightly and highly damped structures, the core loss factor has been assumed to be η_c =0.1 and 1.58, respectively. Figure 5 compares the current results with those proposed in [25], where the capabilities of a refined zig-zag theory were tested for the study of damped structures. A constant harmonic point load (F=1 N) has been applied at the beam tip and the results have been computed at the observation point (b/2, L/2). It can be observed that the amplitudes and phases derived from the LW and the ESL zig-zag theories agree closely with the reference solutions for both loss factors. Conversely, the response predicted by the second-order ESL model is clearly different from the other solutions.

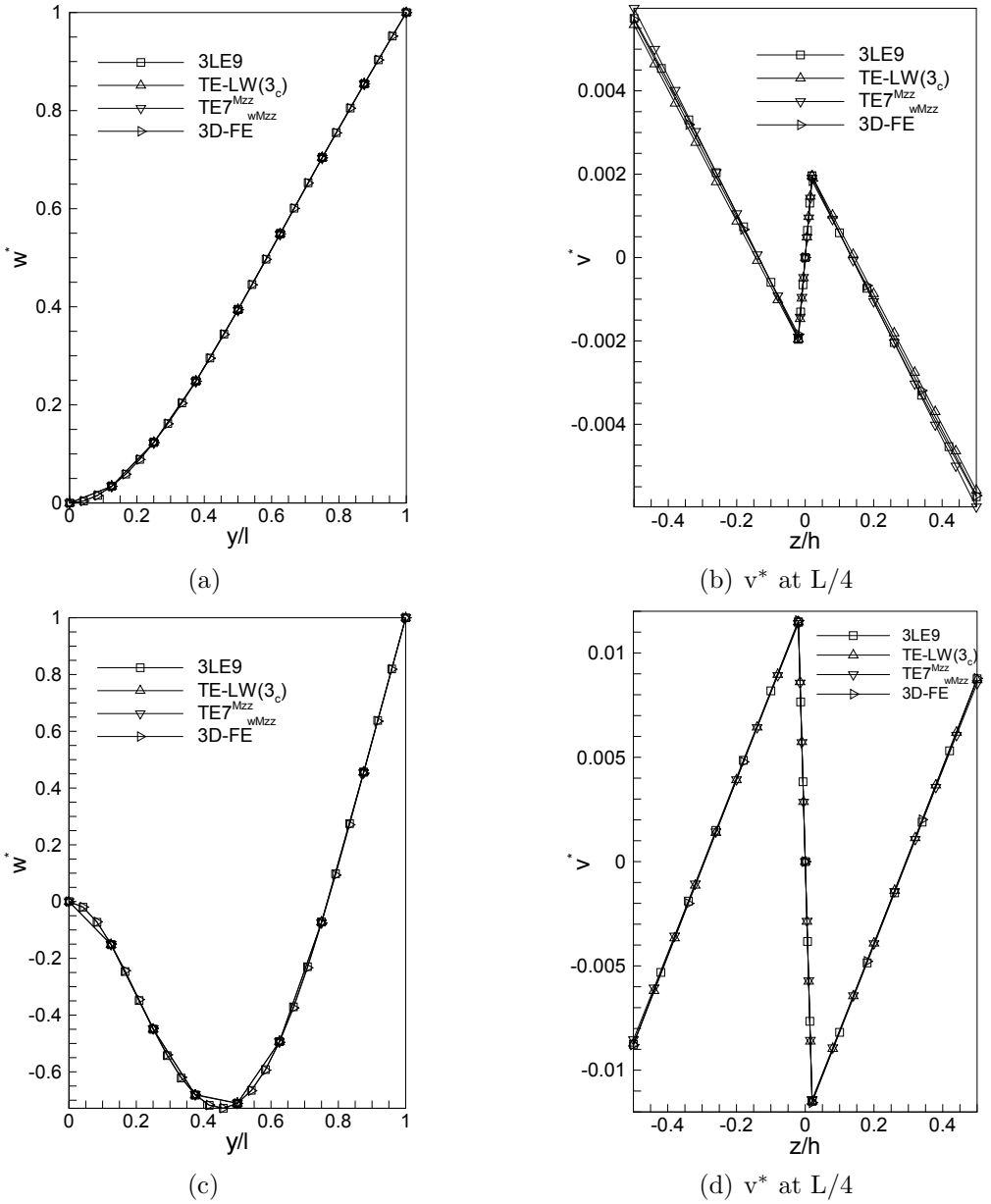

(a) (b) v* at L/4

(c) (d) v* at L/4

Figure 4: Transverse and axial displacement components related to the first and second bending mode shapes. $\eta_c = 1$.

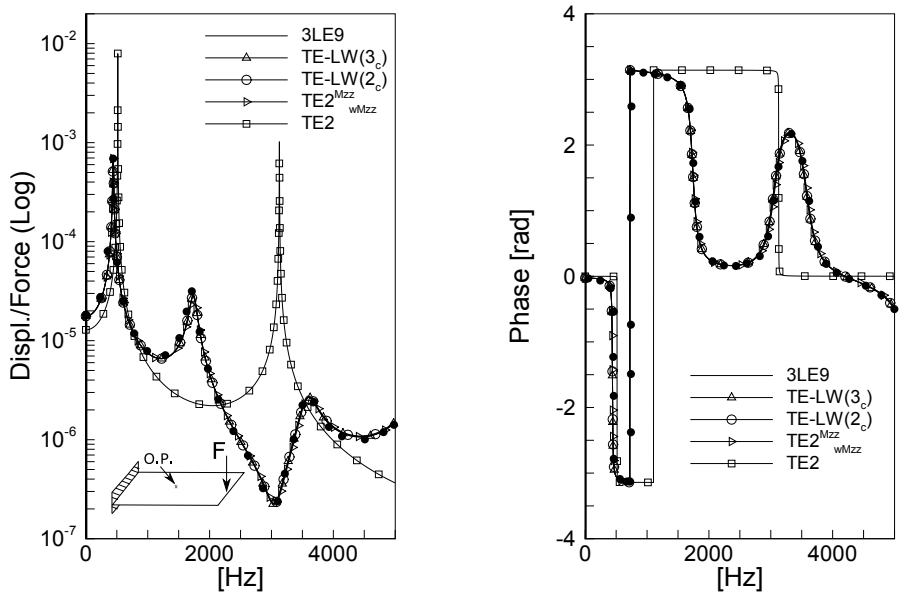

(a) $\eta_c = 0.1$

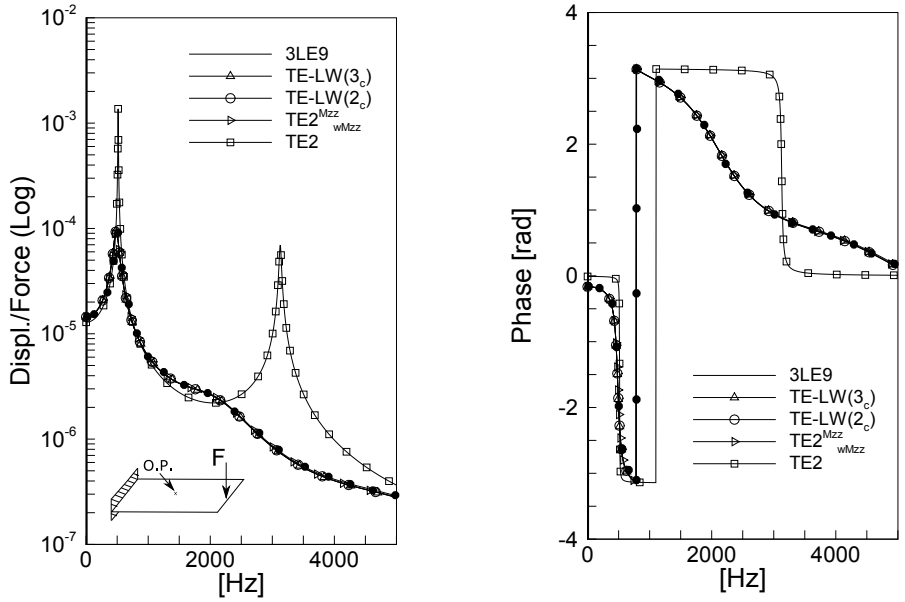

(b) $\eta_c = 1.58$

Figure 5: Amplitude and phase for the sandwich beam subjected to a bending load. '•': numerical solution presented in [25].

Two point loads (F=1 N) have been applied at the beam tip corners to evaluate the torsional response. The amplitude and phase of the observation point (O.P.) are shown in Fig. 6 assuming $\eta_c = 0.1$. Comparisons have revealed that Lagrange-type and TE-LW models provide similar amplitude and phase variations. In particular, the TE-LW(3_c) and 3LE9 curves almost overlap within the considered frequency range (0-5000 Hz). As far as the ESL approach is concerned, it has been found that the warping zig-zag function is mandatory to describe the torsional kinematics properly. In fact, in this case, the Murakami zig-zag term does not produce tangible improvements in the results in comparison to the ESL solution (not reported).

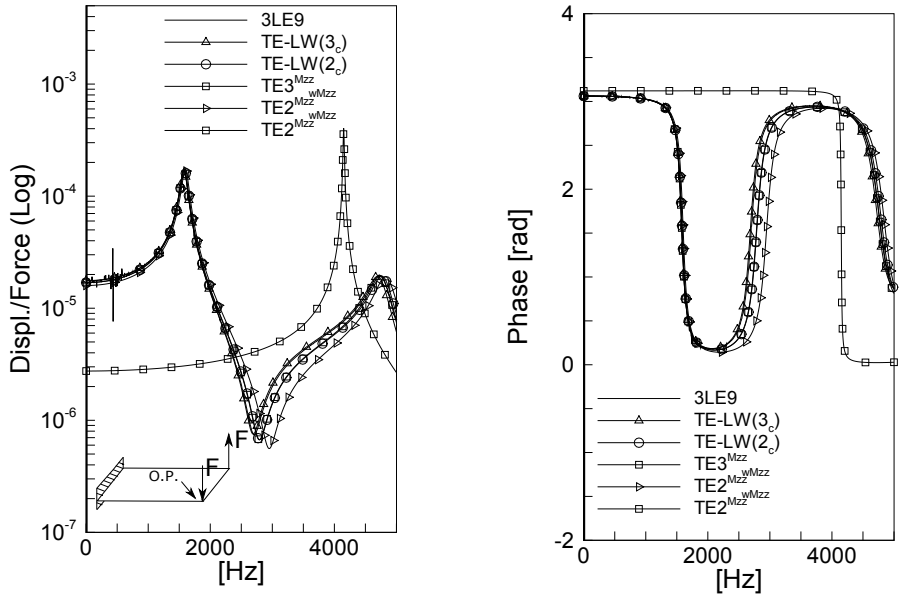

Figure 6: Amplitude and phase for the sandwich beam subjected to a torsional load.

4.3. Asymmetric damped beams

The structure consists of three layers which, starting from the bottom, have the following thicknesses: h_{f1}=1.2, h_c=0.1016 and h_{f3}=0.8 mm. The beam length and width are assumed to be $L = 300$ and $b = 50$ mm, respectively. The external

layers are made out of aluminium (E$_f$=64 GPa, $\nu_f = 0.32$ and $\rho_f = 2695$ Kg m^{-3}) whereas the shear modulus of the thin core ($\nu_c = 0.49$ and $\rho_c = 1000$ Kg m^{-3}) has been assumed frequency-dependent, according to the following viscoelastic laws

$$
\begin{aligned}
G_c &= 2.783 - \frac{1.023}{z_G} \text{ MPa with } \mathrm{z_G} = 0.394 + 0.0003736\mathrm{f} \\
\eta_c &= 1.683 + \frac{0.001468}{z_\eta} - \frac{0.5274}{z_\eta^{0.25}} \text{ with } \mathrm{z}_\eta = 0.005 + 0.0006134\mathrm{f}
\end{aligned}
$$

where f (Hz) is the natural frequency. Figure 7 shows the flexural vibration amplitude and phase of the point ($b/2$, L, 1.0508), where a unit harmonic load is exerted. Unlike previous cases, the higher-order ESL zig-zag solutions are extremely different from the LW results. The discrepancies are essentially due to the different geometrical properties of the face sheets. In fact, Murakami-type zig-zag functions establish a relationship between the layer thicknesses, since they range from -1 to 1, regardless of which layer is considered. In the case in point, the displacement slope should be equal for both face sheets since their material properties are equal. Murakami-type functions have been substituted with linear TE-LW terms, defined over the core subdomain, in order to impose the "same-slope" condition. The related results, which are shown in Fig.7 using the wzz subscript and the zz superscript, demonstrate the effectiveness of the modified zig-zag functions, which have provided accurate estimations of frequencies and modal loss factors.

As far as the LW approach is concerned, it can be observed that the LE and TE-LW theories are in close agreement with each other.

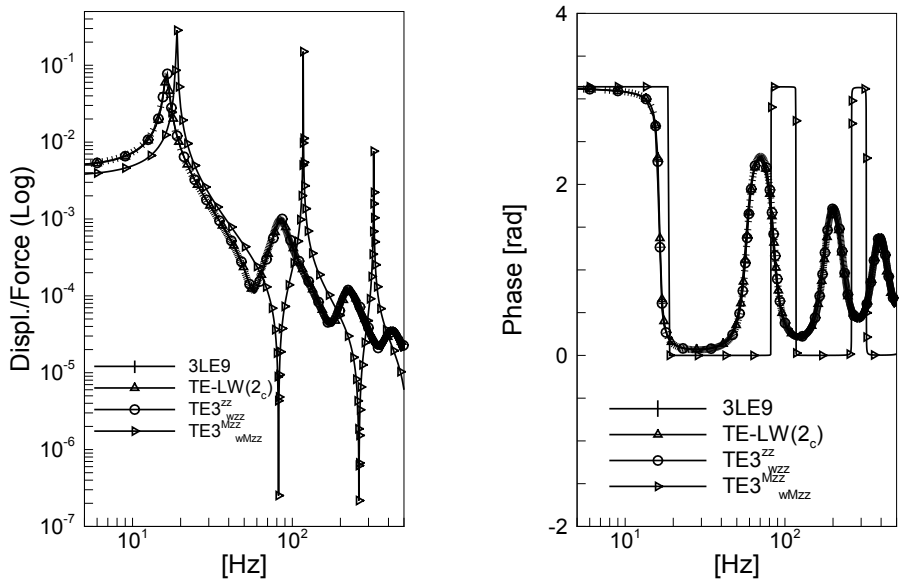

Figure 7: Amplitude and phase for the asymmetric sandwich beam subjected to a bending load.

4.4. Damped rings

Two unconstrained layered rings have been considered to evaluate the 1D-CUF element capabilities for the study of arbitrary-shaped viscoelastic structures. Previous analyses, which were carried out on "rectangular" beam configurations, demonstrated that the ESL-ZZ, TE-LW and LE results were almost coincident. However, the derivation of zig-zag theories might not be a straightforward procedure for "complex" geometries. For this reason, only Lagrange-type elements have been used to model the cross-sections of the rings. Figure 8 shows the adopted mathematical model, which consists of 3 and 20 LE9 elements along radial and circumferential directions, respectively, and a single 3-node beam element along the longitudinal axis. The dimensions and viscoelastic laws of the rings are reported in Tab. 3.

The time-harmonic forced responses of both structures are shown in Fig. 9 and 10, respectively. The results are reported in terms of the loaded point mechan-

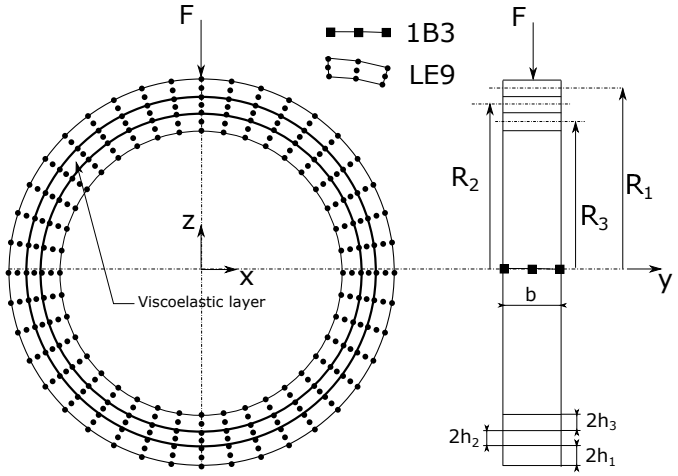

Figure 8: The viscoelastic ring.

	Ring 1	Ring 2
R_1 mm	130.175	110.587
h_1 mm	6.35	0.9487
h_2 mm	5.49	0.0508
h_3 mm	6.35	3.175
b mm	25.4	50.8
ρ_1 kg m^{-3}	7850	7850
ρ_2 kg m^{-3}	2137	1100
ρ_3 kg m^{-3}	7850	7850
E_1 GPa	206	206
E_3 GPa	206	206
ν_1	0.3	0.3
ν_2	0.4	0.4
ν_3	0.3	0.3
G_2 MPa	$3.75\, f^{\,0.50}$	$0.141\, f^{\,0.494}$
η_2	$0.0905\, f^{\,0.288}$	1.46

Table 3: Ring dimensions and material properties.

ical impedance (Force/Velocity) in order to compare the current solutions with those proposed in [37], where an analytical formulation was validated by means of comparisons with experimental data.

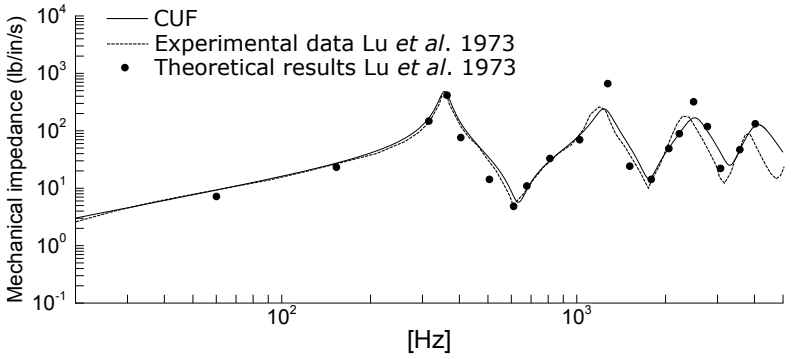

Figure 9: Mechanical loaded point impedances of Ring 1 (1 lb/in/s = 175.13 N/m/s).

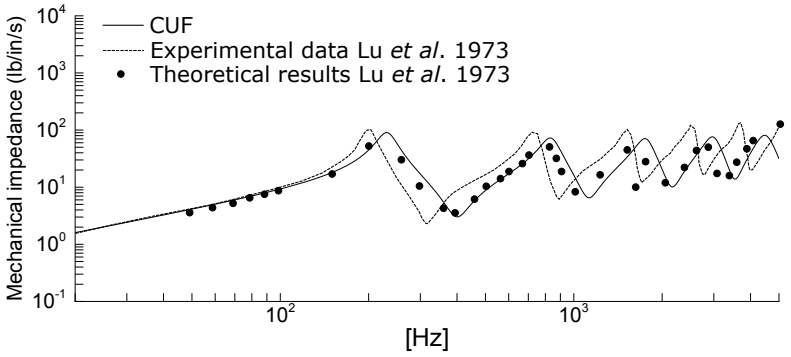

Figure 10: Mechanical loaded point impedances of Ring 2 (1 lb/in/s = 175.13 N/m/s).

Figure 9 indicates that the present results compare well with experimental data within the considered frequency range (20-5000 Hz). As far as the second structure is concerned, the 1D-CUF model predicts higher values of the resonant frequencies than the experimental data, in a similar way to the theoretical reference solution. It is likely that the present finite element solution could be improved further by using a finer cross-sectional mesh.

5. Conclusion

This paper has been aimed at comparing different classes of kinematic theories for the study of passively damped structures. The governing equations, which have been derived by means of the Principle of Virtual Displacement, have been solved using the Finite Element Method. All the mathematical operators (matrices and vectors) related to the different kinematic theories were obtained through the Carrera Unified Formulation. Dynamic analyses were performed on structures with rectangular and circular laminated cross-sections. In light of the obtained results reported in terms of damped frequencies and harmonic responses, it is possible to draw the following conclusions:

- higher-order ESL theories are not able to correctly predict the dynamic characteristics of typical viscoelastic structures;
- the Murakami-type functions represent effective solutions for the prediction of bending and torsional damped frequencies of symmetrical laminated configurations;
- the considered TE-LW theories provided accurate results for asymmetric and symmetric configurations with rectangular cross-sections;
- the LE approach was able to reproduce the reference solutions, regardless of which geometries were considered.

The possibility of adopting a broad range of kinematic assumptions is clearly a valuable feature of the 1D-CUF elements. The presented methodology can be considered a reliable alternative to the commonly adopted modelling techniques, which require a combination of beam, shell and brick elements.

References

[1] D. Roylance. Engineering viscoelasticity. *Department of Materials Science and Engineering–Massachusetts Institute of Technology, Cambridge MA*, 2139:1–37, 2001.

[2] L. Rouleau, J.-F. Deü, A. Legay, J.-F. Sigrist, F. L. Lay, and P. M.-Curtoud. A component mode synthesis approach for dynamic analysis of viscoelastically damped structures. In *Proceedings of the 10th World Congress on Computational Mechanics (WCCM 2012)*, volume 229, page 231, 2012.

[3] E. Barkanov, E. Skukis, and B. Petitjean. Characterisation of viscoelastic layers in sandwich panels via an inverse technique. *Journal of sound and vibration*, 327(3):402–412, 2009.

[4] J. C. Slater, W. K. Belvin, and D. J. Inman. A survey of modern methods for modeling frequency dependent damping in finite element models. In *Proceedings-spie the international society for optical engineering*, pages 1508–1508. Spie international society for optical, 1993.

[5] S. H. Zhang and H. L. Chen. A study on the damping characteristics of laminated composites with integral viscoelastic layers. *Composite Structures*, 74(1):63–69, 2006.

[6] J.S. Moita, A.L. Araújo, C.M. Mota Soares, and C.A. Mota Soares. Finite element model for damping optimization of viscoelastic sandwich structures. *Advances in Engineering Software*, 66:34–39, 2013.

[7] A.J.M. Ferreira, A.L. Araújo, A.M.A. Neves, J.D. Rodrigues, E. Carrera,

M. Cinefra, and C.M. Mota Soares. A finite element model using a unified formulation for the analysis of viscoelastic sandwich laminates. *Composites Part B: Engineering*, 45(1):1258–1264, 2013.

[8] F. Abdoun, L. Azrar, E.M. Daya, and M. Potier-Ferry. Forced harmonic response of viscoelastic structures by an asymptotic numerical method. *Computers & Structures*, 87(1):91–100, 2009.

[9] M. Bilasse, E.M. Daya, and L. Azrar. Linear and nonlinear vibrations analysis of viscoelastic sandwich beams. *Journal of Sound and Vibration*, 329:4950–4969, 2010.

[10] E. M Kerwin Jr. Damping of flexural waves by a constrained viscoelastic layer. *The Journal of the Acoustical Society of America*, 31(7):952–962, 1959.

[11] R.A. DiTaranto. Theory of vibratory bending for elastic and viscoelastic layered finite-length beams. *Journal of Applied Mechanics*, 32(4):881–886, 1965.

[12] D.J. Mead and S. Markus. The forced vibration of a three-layer damped sandwich beam with arbitrary boundary conditions. *Journal of Sound and Vibration*, 10:163–175, 1969.

[13] M.-J. Yan and E.H. Dowell. Governing equations for vibrating constrained-layer damping sandwich plates and beams. *Journal of Applied Mechanics*, 39(4):1041–1046, 1972.

[14] D.K. Rao. Frequency and loss factors of sandwich beams under various bound-

ary conditions. *Journal of Mechanical Engineering Science*, 20(5):271–282, 1978.

[15] L.L. Durocher and R. Solecki. Harmonic vibrations of isotropic, elastic, and elastic/viscoelastic three-layered plates. *Journal of Acoustical Society of America*, 60(1):105–112, 1976.

[16] B.E. Douglas. Transverse compressional damping in the vibratory response of elastic-viscoelastic-elastic beams. *AIAA Journal*, 16(9):925–930, 1978.

[17] C.L. Sisemore and C.M. Davernnes. Transverse vibration of elastic-viscoelastic-elastic sandwich beams: compression-experimental and analytical study. *Journal of Sound and Vibration*, 252(1):155–167, 2002.

[18] Z. Xie and W. S. Shepard Jr. An enhanced beam model for constrained layer damping and a parameter study of damping contribution. *Journal of Sound and Vibration*, 319:1271–1284, 2009.

[19] S.-W. Kung and R. Singh. Vibratian analyis of beams with multiple constrained layer damping patches. *Journal of Sound and Vibration*, 212(5):781–805, 1998.

[20] S.C. Yu and S.C. Huang. Vibration of a three-layered viscoelastic sandwich circular plate. *International Journal of Mechanical Sciences*, 43:2215–2236, 2001.

[21] Y.P. Lu R.A. DiTaranto and B.E. Douglas. Forced response of a discontinuosly constrained damped ring. *The Journal of the Acoustical Society of America*, 54(1):74–79, 1973.

[22] R. Rikards, A. Chate, and E. Barkanov. Finite element analysis of damping the vibrations of laminated composites. *Computers & structures*, 47(6):1005–1015, 1993.

[23] Y. Koutsawa, I. Charpentier, M. C., E.M. Daya, and M. Cherkaoui. A generic approach for the solution of nonlinear residual equations. part i: The diamant toolbox. *Computer Methods in Applied Mechanics and Engineering*, 198(3):572–577, 2008.

[24] J.-M. Berthelot, M. Assarar, Y. Sefrani, and A. El Mahi. Damping analysis of composite materials and structures. *Composite Structures*, 85(3):189–204, 2008.

[25] D. Mundo A. Treviso and M. Tournour. A c0–continuous rzt beam element for the damped response of laminated structures. *Composite Structures*, 131:987–994, 2015.

[26] H. Altenbach A. Korjakin, R. Rikards and A. Chate. Free damped vibrations of sandwich shells of revolution. *Journal of Sandwich Structures and Materials*, 3:171–196, July 2001.

[27] B. Nennig J.-D. Chazot and A. Chettah. Harmonic response computation of viscoelastic multilayered structures using a zpst shell element. *Computers and Structures*, 89:2522–2530, 2011.

[28] F. Abed-Merain F. Kpeky, H. Boudaoud and E.M. Daya. Modeling of viscoelastic sandwich beams using solidshell finite elements. *Composites Structures*, 133:105–116, 2015.

[29] T. Plagianakos and D.A. Saravanos. High-order layerwise finite element for the damped free-vibration response of thick composite and sandwich composite plates. *International Journal for Numerical Methods in Engineering*, 77(11):1593–1626, 2009.

[30] E. Carrera M. Filippi and A.M. Regalli. Layer-wise analyses of compact and thin-walled beams made of viscoelastic materials. *Journal of Vibration and Acoustics*, 138(6):064501–064509, 2016.

[31] M. Filippi and E. Carrera. Bending and vibrations analyses of laminated beams by using a zig-zag-layer-wise theory. *Composites Part B: Engineering*, 98:269–280, 2016.

[32] E. Carrera, G. Giunta, and M. Petrolo. *Beam Structures. Classical and Advanced Theories.* Wiley, 2011.

[33] E. Carrera and M. Filippi. Variable kinematic one-dimensional finite elements for the analysis of rotors made of composite materials. *Journal of Engineering for Gas Turbines and Power*, 136(9):092501, 2014.

[34] H. Murakami. Laminated composite theory with improved in–plane responses. *Journal of Applied Mechanics*, 53:661–666, 1986.

[35] E. Carrera and M. Petrolo. Refined beam elements with only displacement variables and plate/shell capabilities. *Meccanica*, 47:537–556, 2012.

[36] E. Carrera and M. Petrolo. Refined one-dimensional formulations for laminated structure analysis. *AIAA Journal*, 50:176–189, 2012.

[37] Y.P. Lu, B.E. Douglas, and E.V. Thomas. Mechanical impedance of damped three-layered sandwich rings. *AIAA Journal*, 11(3):300–304, 1973.